Potential energy surfaces and reactive dynamics of Zn(^3P) with H$_2$

Michael R. Salazar and Jack Simons
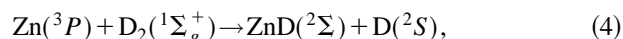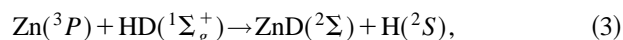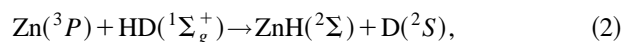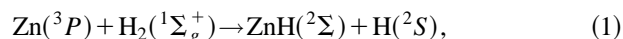
Chemistry Department, University of Utah, Salt Lake City, Utah 84112

The *ab initio* potential energy surfaces pertinent to Zn(^3P)+H$_2$→ZnH($^2\Sigma$)+H have been calculated and are described. For thermal collisions, the dominant reactive surfaces is identified and a mechanism for the reaction on this surface, which may explain the rotational state populations in the ZnH products, is proposed. A novel dynamical technique of running classical simulations on *ab initio* surfaces, using a piecewise tessellation rather than a global functional fit, is briefly introduced with sample trajectories shown. © *1996 American Institute of Physics.* [S0021-9606(96)01648-0]

I. INTRODUCTION

In recent years there has been much experimental attention given to the study of collisional deactivation of electronically excited metal atoms (M) by H$_2$, HD, and D$_2$.[1–8] In these studies, chemical reactivity of the excited metal atom with the isotopic hydrogen has been shown to be the dominant deactivation pathway. A puzzling feature in the MH/MD rotational state populations has been observed in the reactions of Zn($4s4p$, $^3P_1$),[1] Na($4p$, ^2P),[2] Mg($3s3p$, $^1P_1$),[3] Cd($5s5p$, $^3P_1$),[4] and Hg($6s6p$, $^3P_1$).[5] For example, in the exothermic reactions of Zn(^3P), which forms the subject of this paper,

$$\text{Zn}(^3P)+\text{H}_2(^1\Sigma_g^+)\rightarrow\text{ZnH}(^2\Sigma)+\text{H}(^2S), \qquad (1)$$

$$\text{Zn}(^3P)+\text{HD}(^1\Sigma_g^+)\rightarrow\text{ZnH}(^2\Sigma)+\text{D}(^2S), \qquad (2)$$

$$\text{Zn}(^3P)+\text{HD}(^1\Sigma_g^+)\rightarrow\text{ZnD}(^2\Sigma)+\text{H}(^2S), \qquad (3)$$

$$\text{Zn}(^3P)+\text{D}_2(^1\Sigma_g^+)\rightarrow\text{ZnD}(^2\Sigma)+\text{D}(^2S), \qquad (4)$$

Breckenridge *et al.*[1] observed appreciable rotational energy deposition in the ZnH/ZnD products, but with populations that seemed to be independent of the mass of the departing atom. Specifically in reactions (1) and (2), the ZnH product rotational state distributions were essentially identical and likewise for reactions (3) and (4) [see Figs. 1(a) and 1(b)]. It is the causation of the rotational state populations of the (1),(2) and (3),(4) reactions that constitute the primary focus of the present study.

Breckenridge suggested[1] that the release of energy into ZnH or ZnD rotation may be the result of anisotropy in the exit channel potential energy surface (PES). A preliminary classical trajectory study employing simple model potentials with moderate anisotropy indicated the qualitative feasibility of this idea,[9] although no clear reason behind the unusual departing-atom-independent rotational level population arises in that study.

The pertinent Zn+H$_2$ potential energy surfaces have been studied before by others using *ab initio* methods, but not in sufficient detail to permit one to carry out dynamical simulations of the reactions and their product rotational state propensities. Specifically, Martinez *et al.* studied Zn, Zn$^+$, and Zn^{2+}+H$_2$ at the multiconfigurational self-consistent field (MCSCF) and multireference configuration interaction (MRCI) level.[10] However, they examined only limited slices through the three dimensional $^3B_2$ PES, which is thought to be most important for reactive events. This information alone is insufficient to permit dynamical simulations or to globally fit the surface.

We have, therefore, more fully investigated the PES for Zn(^3P)+H$_2$($^1\Sigma_g^+$)→ZnH($^2\Sigma$)+H(^2S). By these calculations and subsequent dynamical simulations on the surfaces obtained, we hope to determine the causes of the unusual rotational state populations observed in ZnH and ZnD.[1]

II. COMPUTATIONAL PROCEDURES

A. Electronic structure methods

A second-order Møller–Plesset (MP2) level treatment of this reaction was found to be sufficient for the PES determined to be most likely to produce the reactive M+H$_2$ events. This level of theory was chosen because of its ability to include dynamical electron correlation effects (as perturbations to the dominant configuration) and because of its computational tractability. MCSCF calculations were performed at several geometries on the PES to verify the presence of a dominant electronic configuration throughout the portion of the PES examined, thereby justifying the use of MP2 at general geometries in these ranges.

An *ab initio* effective core potential, taken from the work of Hay and Wadt,[11] was utilized for the $1s$, $2s$, $2p$, $3s$, and $3p$ orbitals of the Zn atom to further reduce the computer time required. The Zn valance basis set was also selected from the work of Hay and Wadt[11] and subsequently augmented by adding d and f primitive Gaussian functions from previous work on the low lying electronic states of Cu, Zn and their ions.[12] This final ($3s2p6d2f/2s2p3d1f$) basis set is summarized in Table I where the ($3s1p$) H basis can also be found.

B. PES exploration

Mapping out the topology of the three surfaces derived from the Zn(^3P)+H$_2$($^1\Sigma_g^+$) asymptote required a large amount of computer time. For near collinear approach of Zn(^3P) to H$_2$, which Fig. 2 illustrates is orbitally allowed, a total of 230 single point energy calculations were performed for both the sigma ($^3\Sigma$) and pi ($^3\Pi$) states. The variables used
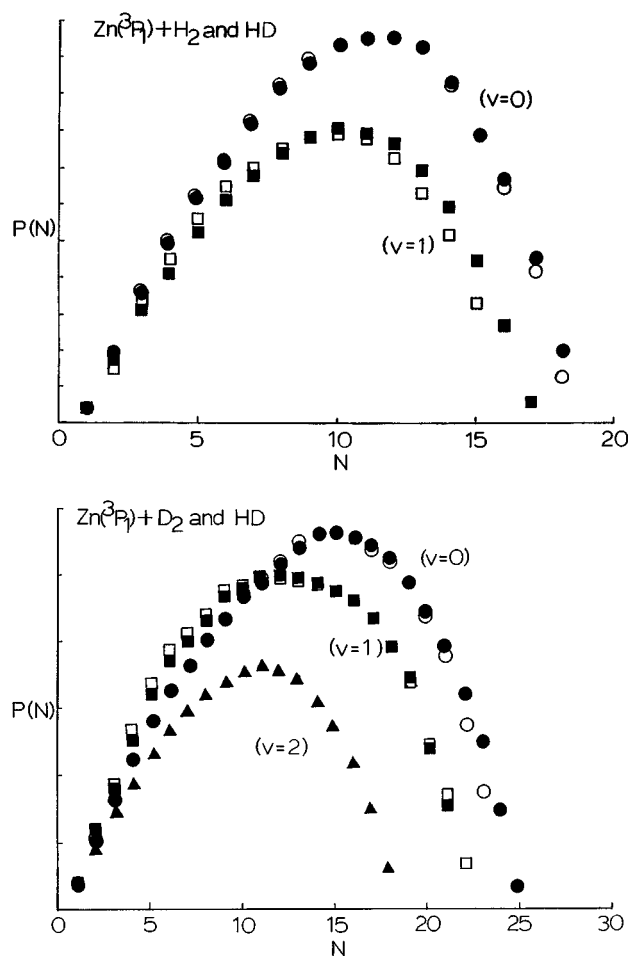
FIG. 1. (a) Rotational quantum state distribution for the reaction of Zn(^3P) with H_2 and HD to form ZnH. Filled circles, squares, and triangles, HD; open circles, squares, and triangles, H_2. (b) Rotational quantum state distribution for the reaction of Zn(^3P) with D_2 and HD to form ZnD. Filled circles, squares, and triangles, HD: open circles, squares, and triangles, D_2.

for collinear calculations are R, the distance from Zn to the nearest hydrogen, and r, the hydrogen-to-hydrogen internuclear distance.

For the near C_{2v} side on approach of Zn(^3P) to H_2, more than 1500 single point energy calculations were performed for the sigma $^3B_2$ surface, 300 single point energy calculations were carried out for the $^3B_1$ surface, and 20 single point energy calculations were carried out for the $^3A_1$ surface. The variables used in these calculations are R, the distance from Zn to the center-of-mass of the H_2 bond, and r, the hydrogen-to-hydrogen internuclear distance.

For the exit channels, connecting to the ground state ZnH($^2\Sigma$)+H(^2S) products, over 3400 single point energy calculations were carried out for the $^3A'$ surface in C_s symmetry. The variables used in these calculations are r_1; the internuclear distance from Zn to the nearest hydrogen atom, r_2; the internuclear distance from Zn to the second hydrogen atom, and theta; the HZnH angle.

C. Calibration studies

Table II shows the results of calculations carried out to test and calibrate the chosen level of theory and basis sets by

TABLE I. Zinc and hydrogen basis sets.

Zinc valence basis set			
s Exponents	Contraction coefficients	p Exponents	Contraction coefficients
0.799 700 021 7[b]	−0.648 611 187 9	0.120 200 000 7[b]	1.0
0.175 200 000 4[b]	1.313 138 290 64	0.035 100 001 8[b]	1.0
0.055 599 998 6[b]	1.0		
d Exponents	Contraction coefficients	f Exponents	Contraction coefficients
68.849 998 47[b]	0.025 853 199 8	2.2[c]	0.424 87
18.319 999 69[b]	0.165 119 499 0	0.55[c]	0.762 88
5.921 999 931[b]	0.446 821 212 8		
1.927 000 046[b]	0.583 108 007 9		
0.552 799 999 7[b]	1.0		
0.180 000 00[c]	1.0		
Hydrogen basis set[a]			
s Exponents	Contraction coefficients	p Exponents	Contraction coefficients
33.865 000 00	0.025 493 800 0	0.750 000 00	1.0
5.094 790 000	0.190 373 000		
1.158 790 000	0.852 161 000		
0.325 840 000	1.0		
0.102 740 000	1.0		

[a]This hydrogen basis consists of five primitive s functions of Huzinaga [J. Chem. Phys. **42**, 1293 (1965)] with the addition of a primitive p function.
[b]Reference 11.
[c]Reference 12.

examining various asymptotes whose energy differences are known experimentally. Note that only the electronic ground state ZnH($^2\Sigma$)+H(^2S) of the product can be formed in thermal collisions of Zn(^3P)+H_2($^1\Sigma_g^+$), and that this reaction is exothermic by 0.2–0.3 eV. This exothermicity limits the rotational and vibrational levels in ZnH and ZnD that can be accessed. In reactions (1) and (2) the ZnH product is limited to v=0,1 and $N\leqslant24,19$, respectively. In reactions (3) and (4) the ZnD product is limited to v=0,1,2 and $N\leqslant31,26,21$, respectively.[1] The ZnH($^2\Pi$)+H(^2S) product lies higher in energy by 2.9–3.0 eV and thus is not accessible in thermal collisions of Zn(^3P)+H_2. Also from Table II it should be clear that, although the features of the various surfaces computed here may be qualitatively correct, they may include errors that may be as large as 0.3 eV.

III. PES RESULTS

A. Near collinear collisions of H_2 with Zn(^3P)

The collinear $^3\Sigma$ energy profile for Zn(^3P)+H_2 is shown in Fig. 3 where, for each R value, r has been energy optimized. Although, it is orbitally allowed and exothermic to form a ZnH($^2\Sigma$)+H(^2S) product via near collinear reactions on the adiabatic $^3\Sigma$ surface, it is energetically impossible for thermal collisions to surmount or penetrate the 0.95 eV barrier leading to a reaction along this surface.

The near collinear $^3\Pi$ reaction of H_2 with Zn(^3P), with configuration $|\sigma^2\sigma\pi|$, correlates adiabatically with ZnH($^2\Pi$)+H(^2S), which is not energetically allowed (see Table II). Hence, the near collinear $^3\Pi$ surface of

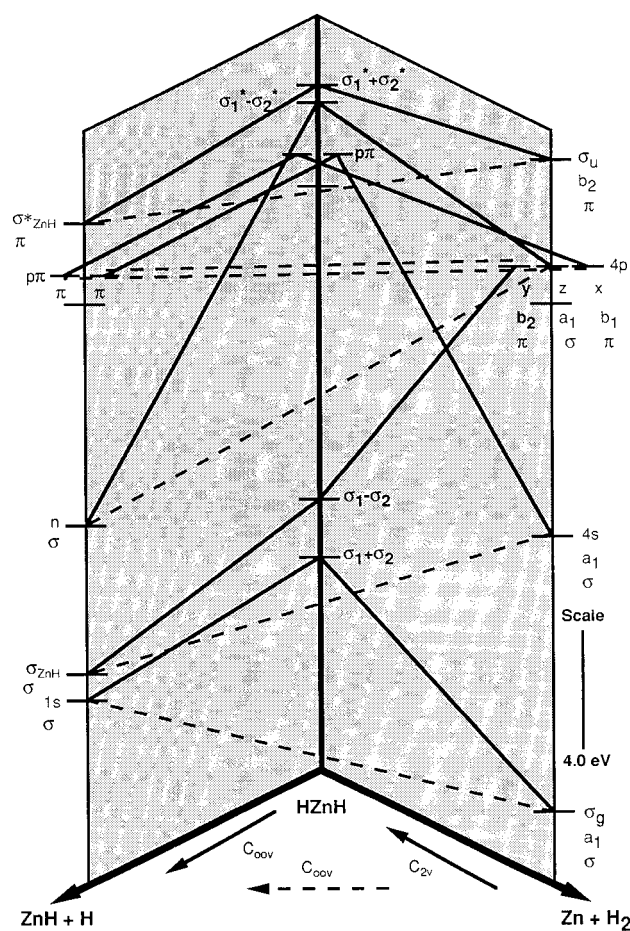FIG. 2. Orbital correlation diagram for Zn+H$_2$. The dashed lines are for the collinear attack of Zn+H$_2$. HZnH corresponds to the fully inserted linear intermediate.

Zn(^3P)+H$_2$ will not be reactive even though, as Fig. 3 shows, this surface is attractive for large R and able to support a bound Zn*···H$_2$ adduct.

For the above reasons, we believe that the near collinear attack of H$_2$ by Zn(^3P) is unfavorable. The barrier for the sigma approach is too high for thermal collisions and would require tunneling of a hydrogen atom through the barrier.

TABLE II. Comparison of the MP2 and experimental thermodynamic energy profiles.[a]

Reaction	ΔE_{Exp} (eV)	ΔE_{MP2} (eV)
Zn(^1S)→Zn(^3P)	4.05[b]	3.79
Zn(^1S)+H$_2$($^1\Sigma_g^+$)→	3.80[b]	3.71
ZnH($^2\Sigma$)+H(^2S)		
Zn(^3P)+H$_2$($^1\Sigma_g^+$)→	−0.25[b]	−0.08
ZnH($^2\Sigma$)+H(^2S)		
ZnH($^2\Sigma$)→ZnH($^2\Pi$)	2.88[b]	3.12
ZnH($^2\Sigma$)→Zn(^1S)+	0.95[c]	0.66
H(^2S)		
Zn(^1S)→Zn$^+$(^2S)+e^-	9.39[c]	9.45

[a]Both energies do not contain zero-point corrections.
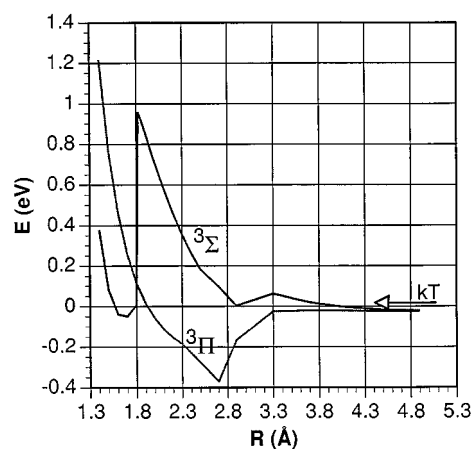[b]Reference 13.
[c]Reference 14.

FIG. 3. Collinear entrance channel; for every R, r was optimized. The energy values in this graph were computed using the MCSCF level of theory. The discontinuities in the gradients are a result of using a course grid of energy points connected by straight lines.

The pi approach adiabatically correlates with an excited state of the product, ZnH($^2\Pi$)+H(^2S), which is not accessible for thermal collisions.

B. Near C_{2v} attack of H$_2$ by Zn(^3P)

1. $^3A_1$ surface

The $^3A_1$ surface with configuration of $|a_1^2a_1a_1|$ diabatically correlates with a doubly excited configuration of the linear product (see Fig. 2) and is found to be repulsive early in the entrance channel (see Fig. 4) as a result of which thermal flux on this surface can not lead to product formation.
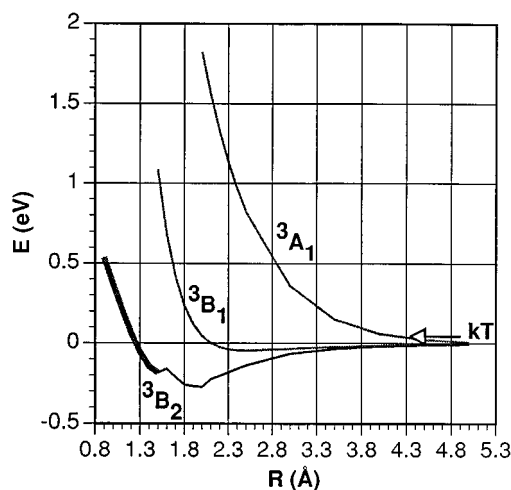

FIG. 4. C_{2v} entrance channel; for every R, r was optimized. The bolder line on the $^3B_2$ surface indicates geometries subsequent to the Δ region introduced in Sec. III B 3. The discontinuities in the gradients are a result of energy points connected by straight lines. However, the barrier at $\sim R=1.6$ Å is real and not a result of a course grid.
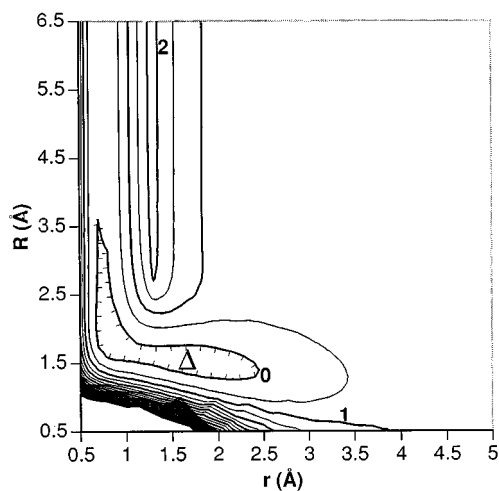
FIG. 5. $^3B_2$ entrance channel contour plot. The Zn*⋯H$_2$ corresponds to the geometry $r = 0.79$ and $R = 1.9$ Å. Units for this plot are eV, with constant contour lines of 0.5 eV, and the zero of energy is the Zn(^3P)+H$_2$ asymptote.

FIG. 6. Exit channel to form ZnH+H. This contour plot shows that it is energetically possible to proceed to product formation. Units for this plot are eV, with constant contour lines of 0.5 eV, and the zero of energy is the Zn(^3P)+H$_2$ asymptote. Theta, the HZnH angle, is fixed at 55.0°.

2. $^3B_1$ surface

The $^3B_1$ surface, with the $|a_1^2 a_1 b_1|$ configuration, diabatically correlates with a doubly excited configuration of the HZnH linear intermediate (see Fig. 2), which is not energetically accessible by thermal flux. Moreover, since the $^3B_1$ configuration has an electron in an out-of-plane orbital, this surface must correlate adiabatically with ZnH($^2\Pi$)+H(^2S), which again is not energetically accessible.

For these reasons, we propose that the $^3B_1$ and $^3A_1$ surfaces are not reactive channels. The $^3A_1$ surface very quickly becomes repulsive early in the entrance channel at geometries where the H$_2$ bond is very much intact. The $^3B_1$ surface, with its out-of-plane electron, can, at best, correlate with the $^2\Pi$ excited state of ZnH.

3. $^3B_2$ surface

The C_{2v} slice through the $^3B_2$ surface shown in Fig. 4, has a minimum corresponding to a Zn*⋯H$_2$ complex which lies ∼0.3 eV below the Zn(^3P)+H$_2$ asymptote. This same surface is shown in two dimensions in Fig. 5 where the narrow entrance channel leading from large R to the Zn*⋯H$_2$ complex is clear.

As seen in Fig. 2, the $^3B_2$ surface can adiabatically correlate with the ground state ZnH($^2\Sigma$)+H($^2\Sigma$) products. This adiabatic correlation is only possible by the ZnH$_2$ complex moving off of C_{2v} symmetry, therefore the PES curvature along the asymmetric stretch coordinate was checked along the thermal-collision-accessible region of the stream bed of the $^3B_2$ entrance channel. What this examination revealed is that in the region near $R = 1.6$ Å, as r is stretched, the PES curvature along the b_2 asymmetric stretch mode diminishes to near zero. In other words, second order Jahn–Teller coupling of the excited $^3A_1$ surface with the $^3B_2$ surface gives rise to this flatness and later negative curvature along the asymmetric stretch in this region of R and r values.
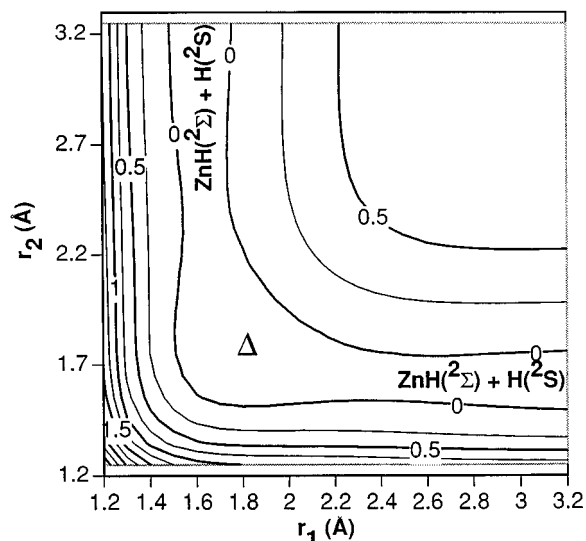
As a result of these findings, the $^3B_2$ state is the surface on which we propose the reaction under study takes place. We suggest that collisional flux on the $^3B_2$ surface proceeds through the entrance valley (within which the H$_2$ bond is essentially intact), through the shallow van der Waals minimum, then proceeds around the "corner" as the H$_2$ bond is breaking and the ZnH bonds are forming. Once the region denoted by Δ in Fig. 5 is reached, the asymmetric stretching mode has softened to an extent that no restoring force exists to overcome even its zero-point bending motion. Figure 6 shows that it is energetically feasible to break one ZnH bond while forming another beginning at geometries near those denoted Δ in Fig. 5. From this region on, the molecule can break C_{2v} symmetry and hence weaken one and strengthen the second of the ZnH bonds and move on to form ZnH+H products.

C. Exit channel

As stated in the Introduction, Breckenridge postulated that the unusual isotope effects in the product rotational state distributions may be due to anisotropy in the exit-channel PES. To test this idea, the $^3B_2$ PES has been characterized, starting near the Δ region of Fig. 5, as a function of the distance (r_2) from Zn to the departing H and θ, the HZnH angle. Such characterization has been made for six values of r_1, the Zn–H distance within the nascent $^2\Sigma$ ZnH molecule, ranging from 1.5 to 1.75 Å, which span the Δ region of Fig. 5 (the r_e of ZnH is 1.6 Å). In Fig. 7, we show one such exit-channel surface cut; those for other r_1 values have similar characteristics. Within the model proposed by Breckenridge, the angular dependence that appears clearly in Fig. 7 in the exit channel causes the ZnH diatomic to rotate as the leaving atom exits.
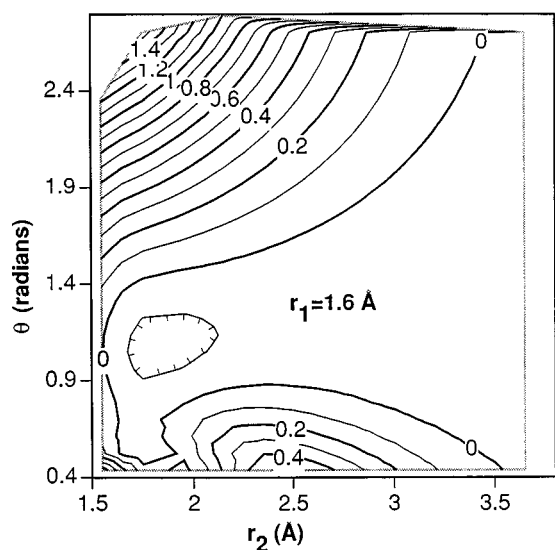
FIG. 7. Contour plot showing the angular dependence of the exit channel. Units are in eV and the zero of energy is the Zn(^3P)+H$_2$ asymptote. Similar exit channels were calculated for r_1 values of 1.5, 1.55, 1.65, 1.7, and 1.75 Å.

IV. PREPARING THE SURFACE FOR DYNAMICAL STUDIES

The primary results achieved in this work include the following:

(1) Calculation of the entrance channel PES for the $^3B_2$ surface of Zn(^3P)+H$_2$ at more than 1500 geometries; along the streambed of the entrance channel analytical energy gradients (i.e., forces) and analytical frequencies have been evaluated.
(2) Identification of the Δ region near which flux can spontaneously evolve away from C_{2v} symmetry and enter the exit-channel leading to ZnH+H products.
(3) Calculation of the exit-channel region of the ZnH($^2\Sigma$)+H surface that connects to the entrance channel near the Δ region noted above. More than 3400 calculations at different geometries were performed to generate the six different (i.e., for six r_1 values) exit-channel surfaces.

As a result, we believe that we now have available a description of the most reactive PES pertinent to the Zn(^3P)+H$_2$→ZnH($^2\Sigma$)+H reaction. To pursue the classical trajectory reactive dynamics simulation aspect of this work, which will be detailed fully in a subsequent paper, we need to have available a representation of our entrance and exit PES's which will allow efficient and accurate computation of the energy and force (gradient) at arbitrary geometries realized in the thermal Zn*+H$_2$ collisions. To this end, and in anticipation of eventually performing quantum dynamics wave function propagation on this same surface, we decided to employ a local piecewise tessellation of the entrance and exit channels together with an interpolation scheme in each tessellation region.

A. Tessellation and interpolation

The tessellation and interpolation method that has been coded in our dynamics routine called UTIMP-PACK (Utah Tessellation Interpolation Multidimensional Propagation Package), consists of the triangulation of the domain (r,R for the entrance channel and r_2, θ for each r_1 value in the exit channel) of the PES and subsequent interpolation of the energy and its derivatives within a given triangle. Since the domain of the PES will admit to many different triangulations, we have chosen to follow a technique that uses so-called barycentric coordinates and a sphere test to construct what is known as Lawson's ''optimal'' triangulation.[15] In essence, the goal of this particular choice of tessellation process is to generate a triangulation in which few ''narrow'' triangles (i.e., those having one very small internal angle) occur and in which triangle areas are similar to one another.

Given a triangulation of the entrance or exit channel region, one next must obtain expressions for the energy and its gradients within each triangle. The methods we use to do so require knowledge of the energy and gradients at each corner of each triangle. In the event that one has not calculated energy gradients at a geometry (hereafter called a node) where one has computed the energy, the missing gradients are generated using the so-called hyperbolic multiquadric method.[16] In the hyperbolic multiquadric interpolant, one employs knowledge of the energy $E(x_j,y_j)$ at $N(j=1,...,N)$ points to determine the N coefficients c_i,

$$E(x_j,y_j)=\sum_{i=1}^{N} c_i[d_i^2(x,y)+r]^{1/2}$$

$$d_i^2(x_j,y_j)=(x_j-x_i)^2+(y_j-y_i)^2,$$

where i runs over the number of nodes included in the interpolation. The parameter r is used to control the weighting of data points close to and far from the point of interest. The gradients are then approximated as

$$\partial E/\partial x=\sum_{i=1}^{N} c_i(x-x_i)[(x-x_i)^2+(y-y_i)^2+r]^{-1/2},$$

$$\partial E/\partial y=\sum_{i=1}^{N} c_i(y-y_i)[(x-x_i)^2+(y-y_i)^2+r]^{-1/2}.$$

Given a triangulation as well as knowledge of the energy and gradients at all nodes, we need to compute these quantities at *any* point inside *any* triangle. To effect this interpolation of the energy and its gradients, we have chosen to use the so-called Clough–Tocher interpolant[17] because it insures the continuity of the energy and gradients (i.e., C^1 continuity) across any triangle boundary as well as continuity of the energy, gradients and second derivatives (i.e., C^2 continuity) inside a triangle when analytical energy and gradient data at the nodes are used. Other multidimensional splinelike interpolants could be employed within each triangle, but we chose to use the Clough–Tocher process for the reasons stated.
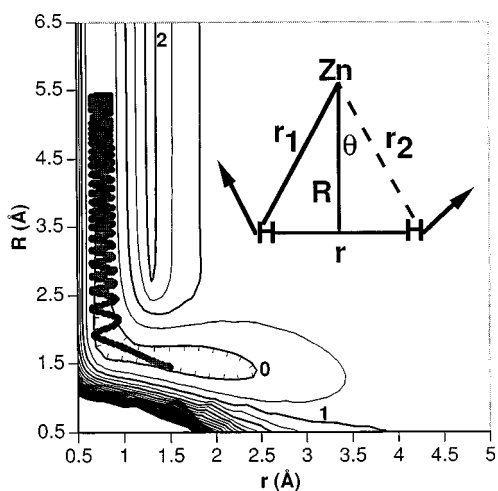
FIG. 8. Entrance channel trajectory suggestive of the collision of Zn(^3P)+H$_2$ at 350 K. The instantaneous velocity vectors for the H atoms at the Δ region are shown.
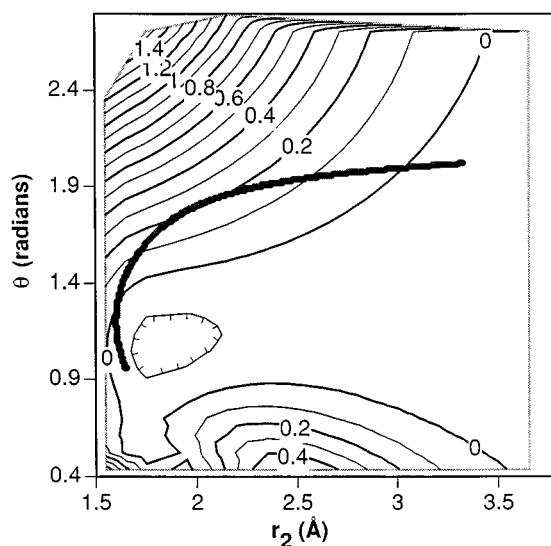

FIG. 9. Exit channel trajectory showing the large angular path taken by the entrance channel trajectory of Fig. 8. The exit channel trajectories are propagated in the center-of-mass coordinates.

B. Suggestive trajectory

A more complete treatment of the ZnH/ZnD product rotational state population must await our completion of the classical trajectory ensemble portion of this work. However, at this time we wish to report preliminary findings that we believe are suggestive. In particular, we display in Fig. 8 a trajectory that results from the following initial conditions that we believe are representative of thermal collisions:

(1) Large R pertinent to Zn(^3P)+H$_2$.
(2) Very small velocity ($\sim$1700 m/s) along R.
(3) Initial H–H distance, r, near the H$_2$ equilibrium distance 0.74 Å.
(4) Momentum along r derived from zero-point energy $h\omega_0/4\pi$ ($p_r^2/2\mu=h\omega_0/4\pi$).

In our simulations when an entrance channel trajectory reaches the Δ region it is halted and the coordinates and momenta are used, together with zero-point energy along the asymmetric stretch mode, as initial values for propagation on an exit channel surface. Also shown in Fig. 8 are the instantaneous velocity vectors of the H atoms in the center-of-mass frame when the above trajectory reaches the Δ region. From these velocity vectors, it is clear that the ZnH$_2$ complex will move off of C_{2v} symmetry to the exit channel C_s symmetry. Clearly, this trajectory moves into the crucial Δ region of the PES with significant momentum along both the r and R axes. Figure 9 shows the exit channel trajectory derived from the entrance channel trajectory of Fig. 8. The coordinates of Fig. 9 are r_2, the Zn to leaving H atom distance, and θ the HZnH angle (although in the exit channel simulations, center-of-mass coordinates are used).

The particular trajectory shown in Figs. 8 and 9 leads to a ZnH product in $v=0$ and $N=13$. An ensemble of such trajectories, representing the thermal collisions realized in the experiment of Breckenridge, must be run and the vibrational and rotational quantum numbers of the ZnH product species binned to more fully simulate these experiments. It is our plan to examine the results of such a classical trajectory swarm to determine whether the origin of the final rotational state populations shown in Figs. 1(a) and 1(b) can adequately be understood. At this time, it seems promising to speculate that torque generated near the Δ region in the entrance channel (see Fig. 8) along with exit-channel surface curvature (see Fig. 9) combine to determine the final N-value of the ZnH product.

ACKNOWLEDGMENT

[1] W. H. Breckenridge and J. Wang, J. Chem. Phys. **87**, 2630 (1987).
[2] S. Billiligin and P. D. Kleiber, J. Chem. Phys. **96**, 213 (1992).
[3] W. H. Breckenridge and J. Wang, Chem. Phys. Lett. **137**, 195 (1987).
[4] W. H. Breckenridge, H. Umemoto, and J. Wang, Chem. Phys. Lett. **123**, 23 (1986).
[5] N. Bras, J. C. Jeannet, and D. Perrin, J. Chem. Phys. **87**, 219 (1987).
[6] W. H. Breckenridge, C. Jouvet, and B. Soep, J. Chem. Phys. **84**, 1443 (1986).
[7] W. H. Breckenridge and H. Umemoto, Adv. Chem. Phys. **50**, 325 (1982).
[8] W. H. Breckenridge, *Reactions of Small Transient Species*, edited by M. Clyne and A. Fontijn (Academic, New York, 1983).
[9] W. H. Breckenridge and J. Wang, Chem. Phys. Lett. **139**, 28 (1987).
[10] J. Martinez-Magadan, A. Ramirez-Solis, and O. Novaro, Chem. Phys. Lett. **186**, 107 (1991).
[11] P. Jeffrey Hay and W. Wadt, J. Chem. Phys. **82**, 270 (1985).
[12] K. K. Sunil and K. D. Jordan, J. Chem. Phys. **82**, 873 (1985).
[13] G. Herzberg, *Molecular Spectra and Molecular Structure*, 2nd ed. (Van Nostrand Reinhold, New York, 1950), p. 579.
[14] C. H. Moore, Atomic Energy Levels, National Bureau of Standards 467, p. 12.
[15] Charles L. Lawson, Comput. Aided Geomet. Design **3**, 231 (1986).
[16] S. Stead, Rocky Mountain J. Math **14**, 265 (1984).
[17] P. Alfeld (personal communication).